Title
Seasonal trace-element and stable-isotope variations in a Chinese speleothem: The potential for high-resolution paleomonsoon reconstruction

Journal
Earth and Planetary Science Letters, 244(1-2)

ISSN
0012-821X

Authors
Johnson, Kathleen R
Hu, Chaoyong
Belshaw, Nick S
et al.

Publication Date
2006-04-15

DOI
10.1016/j.epsl.2006.01.064

Available online at www.sciencedirect.com
SCIENCE DIRECT®
ELSEVIER
Earth and Planetary Science Letters 244 (2006) 394 – 407
EPSL
www.elsevier.com/locate/epsl

Seasonal trace-element and stable-isotope variations in a Chinese speleothem: The potential for high-resolution paleomonsoon reconstruction

Kathleen R. Johnson [a,*], Chaoyong Hu [b], Nick S. Belshaw [a], Gideon M. Henderson [a]

[a] Department of Earth Sciences, University of Oxford, Parks Rd., Oxford, OX1 3PR, UK
[b] Faculty of Earth Sciences, China University of Geosciences, Wuhan, 430074, P. R. China

Received 6 September 2005; received in revised form 18 January 2006; accepted 24 January 2006
Available online 13 March 2006
Editor: H. Elderfield

Abstract

We report the presence of clear annual cycles in trace-element (Mg/Ca, Sr/Ca, Ba/Ca, and U/Ca) and stable-isotope ($\delta^{18}O$ and $\delta^{13}C$) composition in an annually banded stalagmite from Heshang Cave, Hubei Province, China (30.44°N, 110.42°E). Through a combination of micromilling and in situ analysis (LA–MC–ICPMS), we measured geochemical variations across 16 annual growth bands, to assess their potential as seasonal resolution paleomonsoon proxies. To facilitate comparison with modern climatic and environmental data we created composite annual cycles for each proxy by stacking 6 well-defined years. Speleothem $\delta^{18}O$ variations (−10.8‰ to −8.5‰) are controlled by seasonal variations in temperature and drip-water $\delta^{18}O$ which lead to maximum values during May, around the time of summer monsoon onset. This provides a chronological marker which can be used to constrain the timing of the other geochemical cycles. The composite cycles reveal a strong positive correlation between Mg/Ca, Sr/Ca, Ba/Ca, and $\delta^{13}C$ values in the micromilled section (R^2=0.65–0.98), with minimum values occurring around May. Maximum U/Ca values occur at the same time.

We present simple models which show that these correlations, as well as the observed ranges of Mg/Ca (14.1 to 22.4 mmol/mol), Sr/Ca (0.2 to 0.4 mmol/mol), and $\delta^{13}C$ (−12.5‰ to −10.7‰), may be fully explained by progressive CO_2 degassing and calcite precipitation from an initially saturated solution. Using realistic initial conditions for Heshang Cave (T=18 °C, $Mg/Ca_{solution}$=0.84 mol/mol, $Sr/Ca_{solution}$=0.69 mmol/mol, $\delta^{13}C_{TDIC}$=−16.75‰), we find that the observed relationships can be produced by using D_{Mg}=0.016 and D_{Sr}=0.30, within the range of expected values. The model suggests that the fraction of Ca removed from the solution ranges from 0 to 30% to produce the observed seasonal cycles. This variation may be due to two related processes which occur during drier periods: (1) increased prior precipitation of calcite in the epikarst or on the cave ceiling, and/or (2) a greater degree of CO_2 degassing and calcite precipitation on stalagmite surfaces when drip-rates are lower. Both mechanisms would have the effect of enriching speleothem Mg/Ca, Sr/Ca, Ba/Ca, and $\delta^{13}C$ values during drier periods. Past variations in Heshang carbonate chemistry may therefore be useful as seasonal resolution proxies for past rainfall.

Keywords: speleothem; Asian monsoon; paleoclimate; carbonates; trace elements; geochemistry; stable isotopes

* Corresponding author. Tel.: +44 1865 282117; fax: +44 1865 272027.
E-mail address: kathleen@earth.ox.ac.uk (K.R. Johnson).

0012-821X/$ - see front matter © 2006 Elsevier B.V. All rights reserved.
doi:10.1016/j.epsl.2006.01.064

1. Introduction

In recent years, numerous speleothem based proxy studies have significantly advanced our understanding of annual-to-decadal scale paleoclimate variability. While the majority of these studies have focused on the use of speleothem stable-isotope variations ($\delta^{18}O$ and $\delta^{13}C$) to reconstruct paleorainfall, paleotemperature, and/or paleovegetation, several recent studies have investigated the paleoclimate proxy potential of annual trace-element variations preserved in speleothems [1–3]. Annual cycles in trace-element composition, a common feature of speleothems [4], may be useful as paleoenvironmental proxy records with seasonal resolution. Such seasonal records can provide powerful insight into the mechanisms driving climate and can have a large impact on paleoclimate research. Reconstructing past climate at seasonal resolution, however, has generally proven difficult as numerous climatic archives lack sufficient temporal resolution and chronological control. Speleothems, in general, are very well suited for high resolution paleoclimate reconstruction, as they experience no bioturbation; have relatively high growth rates compared to marine sediments; tend to be very well preserved; and can be precisely dated using U-series methods.

In order to use speleothem trace-element variations to reconstruct past changes in climate, it is imperative that the proxies are well understood, well calibrated, and rigorously tested in any individual study area, because numerous environmental, climatic and geologic factors may affect the chemistry of speleothem calcite. Because the incorporation of different elements may have different environmental controls, it is desirable to use a multi-proxy approach to separate these mechanisms to obtain robust seasonal resolution speleothem records. In this study, we assess the potential for seasonal resolution paleoclimate reconstruction from annual geochemical cycles preserved in an annually banded stalagmite, HS-4, collected from Heshang Cave, China (30.44°N, 110.42°E; Fig. 1). HS-4 grew during the last 9.5 kyr and exhibits annual cycles in multiple geochemical proxies. We have performed an ultra-high-resolution study of the stable-isotope ($\delta^{18}O$ and $\delta^{13}C$) and trace-element (Mg/Ca, Sr/Ca, Ba/Ca, U/Ca) composition across 16 annual growth bands to investigate the nature of these geochemical cycles. Based on the comparison of the observed annual cycles with modern calcite, drip water, climatic data, and a simple model, we suggest that annual trace-element (Mg/Ca, Sr/Ca, Ba/Ca, and U/Ca) and stable-isotope ($\delta^{13}C$ and $\delta^{18}O$) cycles record past hydrologic changes which directly reflect past variations in summer monsoon rainfall.

2. Background

The development of quantitative paleoclimate records based on geochemical variations preserved in speleothems is a major goal of recent research. To this end, a number of recent studies have focused in detail on the complicated mechanisms through which trace elements and stable isotopes are incorporated in speleothem calcite [2–9]. Mg incorporation into cave calcite, for instance, is influenced by more than one variable and

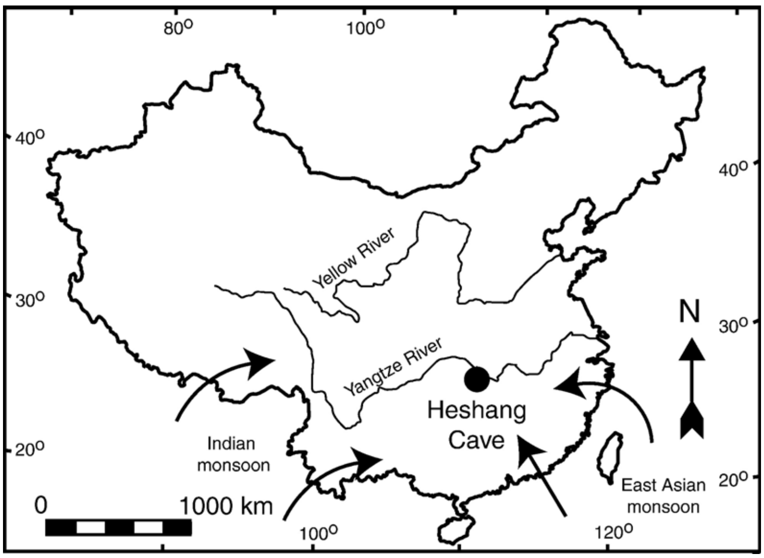

Fig. 1. Location of Heshang Cave. Arrows show a schematic representation of summer monsoon winds.

the relative importance of these variables for the specific location of interest must be understood. More specifically, Mg/Ca of calcite is a function of temperature and the Mg concentration of the solution from which calcite precipitates [10]. Huang and Fairchild [11] measured the partitioning of Mg into calcite under karst-analogue conditions and reported a partition coefficient, D, where $D_{Mg} = (Mg/Ca)_{calcite}/(Mg/Ca)_{solution}$ equal to 0.031 ± 0.004 at 25 °C and 0.019 ± 0.003 at 15 °C. Temperature in most deep caves, however, is constant and equal to the mean annual surface temperature throughout the year [12], therefore Mg/Ca variations in speleothem calcite are usually controlled by variations in the Mg/Ca ratio of cave drip water.

Four possible mechanisms have been proposed to explain annual Mg cycles in cave drip waters [6]: (1) Calcite dissolves at a faster rate than dolomite [13,14], therefore, increased residence time during drier periods may allow for more dissolution of dolomite, leading to higher Mg/Ca ratios in cave drip waters. (2) Prior calcite precipitation due to CO_2 degassing in the epikarst or on the roof of caves will lead to an increase in Mg/Ca of cave drip waters, because $D_{Mg} \ll 1$ [15]. This mechanism should lead to similar annual cycles in other trace elements with $D \ll 1$ (Sr, Ba, etc.), and also in $\delta^{13}C$, due to the preferential release of ^{12}C into degassed CO_2 during the prior precipitation. (3) Incongruent dolomite dissolution, in which Ca is preferentially released from fresh dolomite surfaces, could lead to increased drip-water Mg/Ca with increased residence time, but this mechanism is not thought to be significant in most cases [16]. A related mechanism which may lead to increased Mg/Ca occurs when dolomite dissolution leads to calcite supersaturation and precipitation. The resulting Mg/Ca increase in this case is related to prior calcite precipitation (mechanism 2). (4) Selective leaching of Mg (and Sr) may occur if there is an easily leached non-carbonate source of excess Mg and Sr or if incongruent calcite dissolution occurs [17]. For example, Mg may be released as Mg-calcite transforms to low-Mg calcite.

Sr (and Ba) incorporation into calcite is unaffected by temperature variations, but is weakly dependent on crystal growth rate, in addition to in the chemistry of the drip water[15,18]. Huang and Fairchild measured D_{Sr} values that range from about 0.057 to 0.078 [11]. Because the incorporation of both Mg and Sr into calcite is governed by D values that are less than 1, co-variation of Mg and Sr in speleothems is an indicator that prior calcite precipitation is the dominant mechanism.

Annual U and P cycles are thought to have somewhat different controls. U and P tend to co-vary in groundwaters, because there is a strong affinity between phosphate and uranyl ion. P variations in a modern speleothem exhibit a strong positive correlation with rainfall, most likely related to seasonal vegetation decay and the resulting pulse of P as HPO_4^{2-} [3]. In addition, during prior calcite precipitation, P, and possibly U, is very strongly scavenged out of groundwater onto mineral surfaces [4].

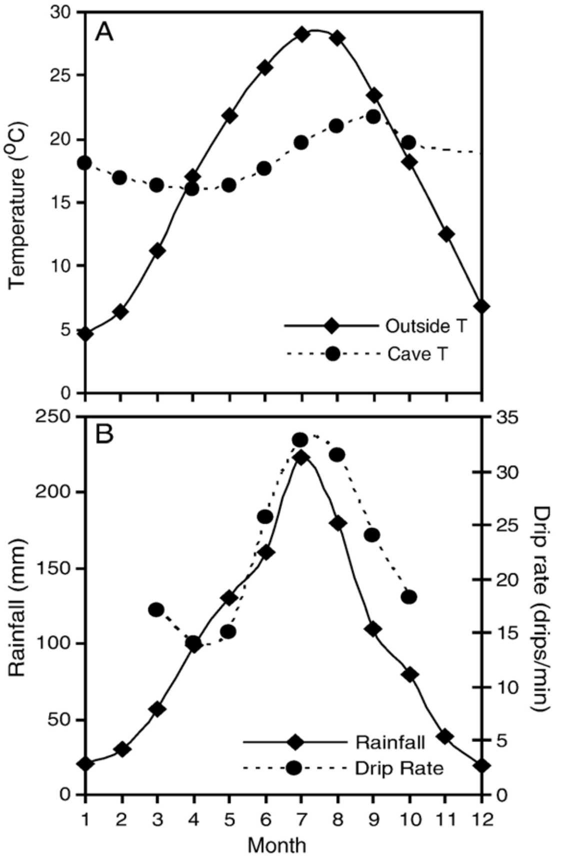

Fig. 2. Modern climate data for Yichang, China (30.70°N, 111.30°E), obtained from the Global Historical Climatology Network, and cave environment data from Heshang Cave. (A) Mean monthly temperature record for outside the cave (Yichang data, average of 654 months from 1924 to 1991), and inside the cave near the HS-4 collection site. (B) Mean monthly rainfall data for the Heshang Cave region (Yichang data, average of 1174 months from 1882 to 1988), and mean monthly drip-rates measured at the HS-4 collection site.

3. Environmental setting

The study area, Heshang Cave, is located at an elevation of 202 m in the Qingjiang valley in southern China (Fig. 1), near the central Yangtze River valley. The cave extends approximately 250 m from a single large entrance, and is overlain by 300 m of Cambrian dolomite. The area is covered by a well-developed 40-cm-thick layer of soil derived from the dolomite bedrock,

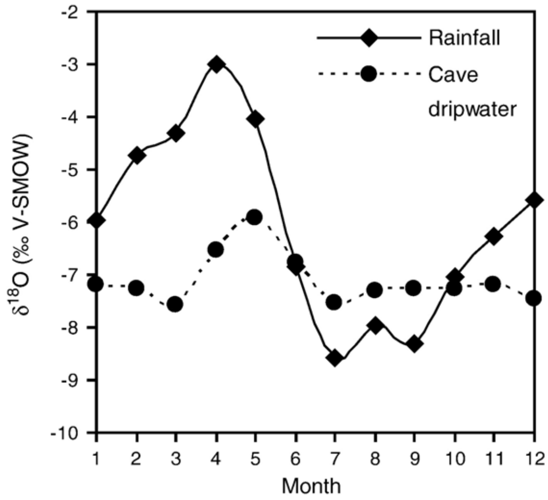

Fig. 3. Mean monthly rainfall and Heshang Cave drip-water $\delta^{18}O$. Rainfall $\delta^{18}O$ values are modelled data as calculated from the Online Isotopes in Precipitation calculator (http://www.waterisotopes.org) [19,20] using Heshang Cave latitude, longitude, and elevation. Drip-water $\delta^{18}O$ values are the average of 2–3 samples per month collected at the HS-4 collection site.

wind-blown silicate dust, and organic matter from the dense local vegetation.

The highly seasonal climate of the study area is dominated by the East Asian monsoon system. The mean annual temperature is ≈ 18 °C, with daily averages ranging from 5 °C to 28 °C (Fig. 2A), and the mean annual precipitation is ≈ 1460 mm, with approximately 80% of the annual rainfall occurring during the summer monsoon months of June, July, and August (Fig. 2B). Relative humidity in the deeper parts of the cave is > 95% throughout the year. The modern Heshang Cave environment responds rapidly to seasonal changes in temperature and rainfall. Temperature recorded by data loggers in Heshang Cave from September 2003 to April 2005 indicate that, unlike many caves, temperature inside Heshang Cave does vary, ranging from 16 °C to 22 °C throughout the year (Fig. 2A). This damped annual temperature cycle lags the outside surface temperature cycle by 2–3 months. Likewise, drip rate measurements, conducted 2–3 times per month between March and November 2004 at the former site of HS-4, indicate a rapid response to rainfall at the surface. Drip rate increases abruptly in May, coincident with the onset of the summer monsoon rainfall.

The oxygen-isotope composition of HS-4 drip water also responds rapidly to changes in rainfall composition. The average $\delta^{18}O$ of rainfall at Heshang Cave, calculated using the Online Isotopes in Precipitation Calculator [19,20], varies between −3.0‰ in April and −8.6‰ in July (Fig. 3). The most negative values are seen during the summer monsoon months, indicating that the amount effect on $\delta^{18}O$ of rainfall dominates over the temperature effect [21,22]. Heshang Cave speleothem oxygen-isotope variations are, therefore, a useful proxy for the amount of monsoon precipitation. Heshang Cave drip-water has a damped and lagged response to changes in rainfall $\delta^{18}O$ (Fig. 3; Hu et al. [47]). The maximum drip-water $\delta^{18}O$ occurs in May, 1 month after the peak in rainfall $\delta^{18}O$ and, around the time of summer monsoon onset when rainfall and drip rate rapidly increase. This suggests that the initial increase in drip rate, most likely due to an increased hydraulic head and/or increased fracture flow with the onset of monsoon rainfall, forces through older rainwater that was stored in the epikarst for at least 1 month. The damped nature of the drip-water $\delta^{18}O$ cycle indicates the occurrence of mixing in the epikarst, but the structure of the seasonal cycle requires that the average transit time is less than 1 yr.

4. Methods

4.1. Microsampling

We selected a 7-mm-long section of stalagmite HS-4 from the early–mid Holocene (~7 ka) which is characterized by clear annual growth bands, each band consisting of a light–dark couplet (Fig. 4). We chose this sample due to its quite parallel and laterally continuous growth bands, and generally low porosity, thus facilitating accurate microsampling and in situ analysis on the same section. We used a New Wave Research

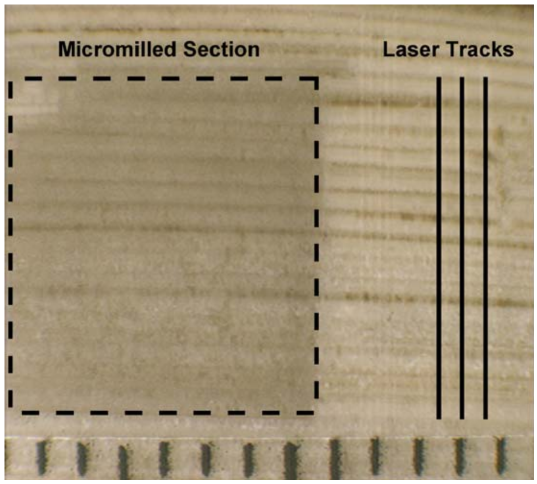

Fig. 4. The section of the stalagmite, HS-4, used for this study. This section, which formed at ~7 ka, was chosen for its relatively parallel growth bands and the range of thicknesses and color represented. The tick marks on the ruler at the bottom are spaced at 1-mm intervals.

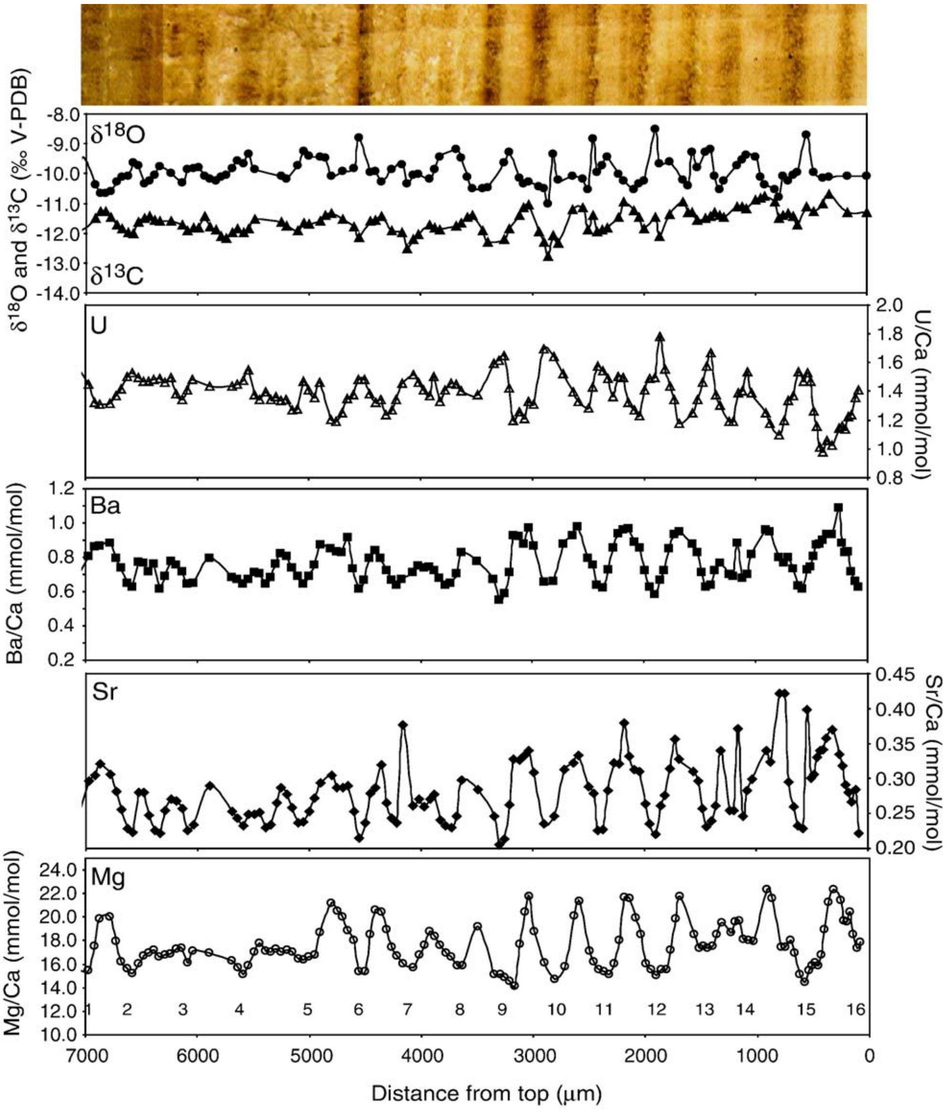

Fig. 5. Plots of annual trace element (U, Ba, Sr, and Mg) and stable-isotope ($\delta^{18}O$ and $\delta^{13}C$) cycles measured on micromilled samples plotted versus distance from the top (youngest samples to the right). The stalagmite section sampled is shown above for comparison. The Mg troughs were used to define 16 years, which are numbered at the bottom. Years 7–12 were stacked to develop the composite record (Fig. 7).

Micromill to collect 160 samples across an approximately 7×7 mm^2 section of the sample. We utilized a milling technique whereby an initial 150 µm deep trench was milled parallel to the growth banding. The spatial resolution of this initial sample was limited by the thickness of the drill bit (~0.3 mm). After milling this initial trench, however, the growth bands were sampled by progressively moving the drill path in ~44-µm steps, parallel to the growth bands, thus essentially shaving off 44-µm-thick samples throughout this section, resulting in a final sampled volume of about 0.05 mm^3 and an average sample mass of about 120 µg. The samples were collected with a scalpel and subsequently split evenly into two 1.5-ml microcentrifuge tubes for stable-isotope and trace-element analysis.

4.2. Stable-isotope analysis

Samples were measured at UC Berkeley, where 20–50 µg of carbonate was reacted with phosphoric acid at 90 °C for 15 min. The released CO_2 gas was transferred through a water trap and then measured on a GV Isoprime mass spectrometer. Oxygen and carbon isotopic data are reported in the δ notation relative to the V-PDB standard for carbonate samples and the V-SMOW standard for water samples, where $\delta=[(R_{sample})/(R_{std})-1]\times 1000$, and $R={}^{18}O/{}^{16}O$ for oxygen and ${}^{13}C/{}^{12}C$ for carbon. The precision for each analysis is ±0.05‰ for carbon and ±0.06‰ for oxygen.

4.3. Trace metal analysis via ICPMS

Mg/Ca, Sr/Ca, Ba/Ca, and U/Ca ratios were measured using the "ratio" method [23,24] on a Perkin Elmer Elan ICPMS. Samples were dissolved in 2% distilled HNO_3 and diluted so that Ca concentrations were equal to that of the external, matrix-matched standard (30–70 ppm Ca). Element/Ca ratios were calculated directly from intensity ratios, using a standard bracketing technique to correct for instrumental mass discrimination. Average precision (1σ) is 0.39% for Mg/Ca, 0.65% for Ba/Ca, 0.37% for U/Ca, and 1.37% for Sr/Ca, based on replicate analyses of the matrix-matched standard.

4.4. In situ trace metal analysis via LA–MC–ICPMS

Mg/Ca and Sr/Ca ratios were also measured in situ using a New Wave Research 193 nm ArF pulsed excimer laser ablation (LA) system attached to a Nu Plasma MC–ICPMS. LA analyses were performed adjacent to the micromilled samples (Fig. 4). Numerous runs were performed, testing various configurations of pulse rate, spot size and shape, He sweep-gas flow rate, and scan speed. The results reported in this study utilized a slit shaped 25 μm × 250 μm spot size, a 20 Hz repetition rate, a 5 μm/s scan speed, 0.8 l/min He sweep gas, and a 0.5-s integration time. Mg/Ca ratios were measured by simultaneous collection of mass 24 (${}^{24}Mg^{+}$) and mass 21.5 (${}^{43}Ca^{2+}$). Sr/Ca ratios were measured by simultaneous collection of mass 43.5 (${}^{87}Sr^{2+}$) and mass 44 (${}^{44}Ca^{+}$). The results presented in this study represent the average of 3 laser ablation passes following pre-cleaning by a previous laser ablation scan. For the purpose of this study, we chose not to use a laser ablation standard due to the difficulties of obtaining matrix-matched trace-element standards and the strong matrix dependence of laser-fractionation [25,26]. Instead, Mg/Ca and Sr/Ca ratios were calculated directly from measured ion-beam intensities (corrected for isotopic abundance). Rather than compare true elemental ratios, we normalized all data by the measured average for the scans in order to directly compare the range of element ratios measured by LA–MC–ICPMS with those measured by conventional ICPMS. One major assumption of this method is that a constant proportion of Ca^{2+} is formed in the plasma relative to total Ca (and, likewise, a constant ratio of Sr^{2+} relative to total Sr). Further details of the LA–MC–ICPMS method will be discussed in Johnson et al. [27].

5. Results and discussion

5.1. $\delta^{18}O$

Stable-isotope analysis of micromilled samples reveals clear annual cycles in $\delta^{18}O$ and $\delta^{13}C$ (Fig. 5). $\delta^{18}O$ values range from −10.8‰ to −8.5‰. This range is lower than the expected modern $\delta^{18}O$ range of −8.7‰ to −5.8‰, because higher monsoon intensity in the early Holocene led to more negative $\delta^{18}O$ values in rainfall and, hence, in speleothem calcite [28,29]. Because the $\delta^{18}O$ of speleothem calcite is a function of temperature (−0.24‰/°C), in addition to drip-water $\delta^{18}O$, part of the amplitude of the annual $\delta^{18}O$ cycles may be explained by temperature variations in Heshang Cave. When cave temperatures are lowest in late spring (Fig. 2), coincident with high drip-water $\delta^{18}O$ (Fig. 3), the temperature control on calcite–water fractionation may contribute to high $\delta^{18}O$ calcite precipitated at this time. Conversely, high temperature and low drip-water $\delta^{18}O$ during the late summer and fall lead to calcite with lower $\delta^{18}O$. The observed seasonal $\delta^{18}O$ cycle observed in the stalagmite is, therefore, controlled by a combination of drip-water composition and temperature changes. Because we expect no major changes in the timing of the annual drip-water $\delta^{18}O$ or cave temperature cycle, however, the peak calcite $\delta^{18}O$ should always occur in the late spring.

Based on the modern relationship between $\delta^{18}O$ of rainfall and cave drip water, we expect that the annual peak in $\delta^{18}O$, which sometimes appears as a very sharp change, reflects the isotopically heavier winter rainfall that is quickly flushed through the epikarst at the onset of the monsoon season in May. There is no reason to think that the basic structure of the annual rainfall and drip-water $\delta^{18}O$ cycle was significantly different in the early Holocene. Therefore, we assume that each $\delta^{18}O$ peak represents May and we use this point to anchor the remaining geochemical data to a quasi-seasonal time scale. We are unable to assign calendar months to the remaining data, however, because calcite growth rate may vary throughout the year, for example as modelled by Genty et al. [30].

5.2. $\delta^{13}C$

$\delta^{13}C$ values range from −12.5‰ to −10.7‰ and are uncorrelated with $\delta^{18}O$ values, suggesting that the two

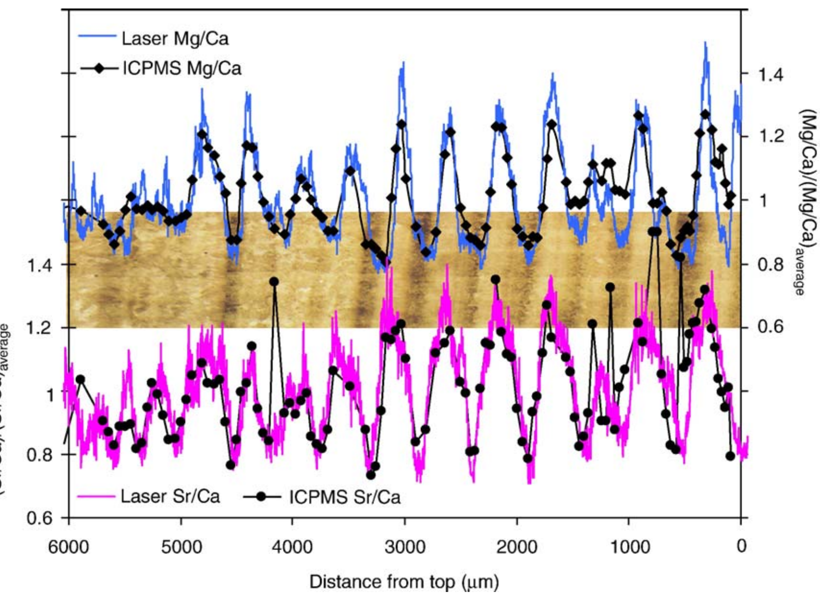

Fig. 6. Comparison between Mg/Ca and Sr/Ca ratios measured on the micromilled HS-4 samples via ICPMS versus LA–MC–ICPMS. The plotted ratios have been normalized to their average to allow direct comparison.

are controlled by different environmental processes. Speleothem $\delta^{13}C$, unlike $\delta^{18}O$, is not significantly affected by temperature [31]. Seasonal variations in $\delta^{13}C$ may, instead, be caused by a number of other factors, including: (1) changes in the ratio of C_3 : C_4 vegetation leading to changes in $\delta^{13}C$ of soil CO_2 [32–34]; (2) changes in the degree of mixing between atmospheric CO_2 and CO_2 derived from root respiration and microbial activity [35]; (3) changes in the degree of open versus closed system dissolution [31,36]; (4) variation in the amount of degassing due to changes in cave air pCO_2 [37]; and (5) changes in the amount of prior calcite precipitation, which may be related to mechanism 4 [35,38].

Seasonal $\delta^{18}O$ variations in speleothems were reported and discussed by Treble et al. [8], whereas seasonal $\delta^{13}C$ variations in speleothems have not been discussed in depth. The presence of seasonal cycles in $\delta^{18}O$ and $\delta^{13}C$ has significant implications for the widespread use of the "Hendy test" for isotopic equilibrium. Hendy observed that kinetic-isotope fractionation during rapid CO_2 degassing and evaporation, would lead to coupled increases in $\delta^{13}C$ and $\delta^{18}O$ of speleothem calcite precipitated along individual growth bands [31]. This observation has led to the widespread application of the Hendy test, by which stable-isotope measurements are made along a single growth band to check that the calcite grew in equilibrium conditions. It is now being acknowledged [8] that such a test, while valid in theory, is quite difficult to perform successfully, because sampling perfectly along an individual growth horizon is extremely difficult. The observation of large amplitude seasonal $\delta^{18}O$ and $\delta^{13}C$ cycles at Heshang cave suggests that such sampling would have to be accurate at seasonal resolution (i.e. on a length scale of tens of microns). Even if sampling of single annual growth bands can be achieved, the likelihood of sampling calcite which actually formed coevally is minimal. The Hendy test may, however, be useful as a test for kinetic-isotope fractionation in situations where speleothem $\delta^{18}O$ does not vary seasonally and/or where several annual layers can be averaged.

5.3. Trace elements

ICPMS analyses of the micromilled samples reveal clear annual cycles in trace-element geochemistry (Fig. 5). Mg/Ca, Sr/Ca, and Ba/Ca ratios are positively correlated with each other (R^2 = 0.28–0.61) as well as with $\delta^{13}C$ (R^2 = 0.38–0.51). U/Ca, on the other hand, is negatively correlated with Mg/Ca, Sr/Ca, Ba/Ca, and $\delta^{13}C$ (R^2 = 0.25–0.36), but exhibits a weak positive correlation with $\delta^{18}O$ (R^2 = 0.19). We define 16 annual cycles (Fig. 5) based on the location of Mg/Ca troughs, which correspond closely to color changes in the micromilled section. Light bands are characterized by higher Mg, Sr, and Ba concentrations, and higher $\delta^{13}C$ than dark bands. Darker bands are characterized by high U concentrations, possibly due to the association of U with organic material which may also be enriched in the darker bands.

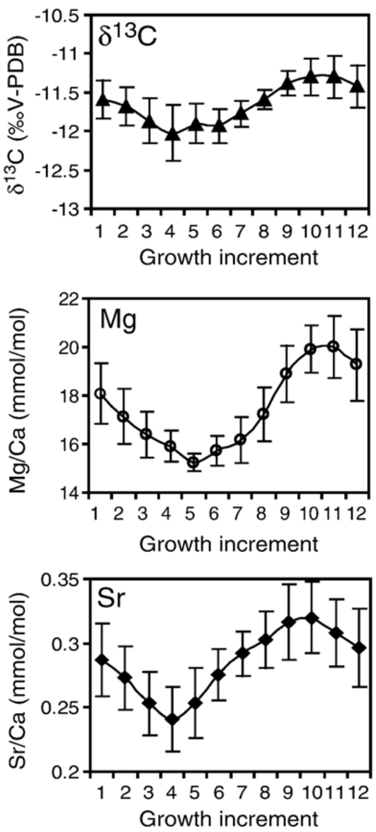

Fig. 7. Composite annual cycles in Mg/Ca, Sr/Ca, Ba/Ca, U/Ca, $\delta^{13}C$, and $\delta^{18}O$. These cycles were calculated by stacking 6 years of the micromilled record (7–12 in Fig. 5). Each year was interpolated to 12 equally spaced points. Each of these points, representing a single growth increment, was averaged for the 6 years to create the composite record. Error bars are 2 standard deviations of the mean of the six values. The growth increments most likely do not correspond to calendar month, as growth rate may vary throughout the year. However, as discussed in the text, increment 5 probably corresponds to May.

LA–MC–ICPMS analyses also clearly reveal the annual cycles in Mg/Ca and Sr/Ca ratios. The normalized laser ablation ratios are extremely similar to the normalized Mg/Ca and Sr/Ca ratios measured by conventional ICPMS (Fig. 6). The small amplitude differences between the two methods may be due to the lesser amount of smoothing that occurs during laser ablation relative to micromilling. The strong similarity between the two different methods suggests that fractionation effects and variation in the proportion of doubly charged Ca and Sr ions produced in the plasma, are small and do not significantly affect the measured ratios.

5.4. Composite annual cycles

Following the approach of Treble et al. [3], we calculated composite annual trace-element and stable-isotope cycles by stacking 6 well-defined yrs from the micromilled time series (years 7–12 in Fig. 5). This method allows us to investigate the general pattern of trace-element and stable-isotope variability, and compare this data to modern temperature (surface and cave), rainfall, drip rate, and drip-water $\delta^{18}O$ cycles. Based on Mg troughs, data from each of the 6 yrs were linearly interpolated to 12 equally spaced points (termed growth increments 1–12), and then the 6 yrs were averaged to create the composite record for each proxy (Fig. 7). This method preserves the phasing between the different geochemical proxies, thus allowing us to more clearly investigate the possible control mechanisms on each one. This averaging process somewhat dampens the amplitudes of the composite Mg/Ca (15.2–20.0 mmol/mol), Sr/Ca (0.2–0.3 mmol/mol), Ba/Ca (0.7–0.9 mmol/mol), U/Ca (1.3–1.5 nmol/mol), $\delta^{13}C$ (−11.3‰ to −12.0‰), and $\delta^{18}O$ (−10.2‰ to −9.4‰) cycles relative to the range observed in the full micromilled section time-series.

In each of the composite cycles, growth increment 5 is considered to represent calcite growth during May, as

Table 1
Summary of correlation coefficients (R^2) between the composite trace element and stable isotope data

	Mg/Ca	Sr/Ca	Ba/Ca	U/Ca	$\delta^{18}O$	$\delta^{13}C$
Mg/Ca	1	0.65	0.72	−0.85	−0.62	0.93
Sr/Ca	–	1	0.98	−0.56	−0.31	0.81
Ba/Ca	–	–	1	−0.68	−0.40	0.85
U/Ca	–	–	–	1	0.63	−0.82
$\delta^{18}O$	–	–	–	–	1	−0.44
$\delta^{13}C$	–	–	–	–	–	1

constrained by the timing of the $\delta^{18}O$ peak. The other growth increments, however, may or may not correspond to calendar months, depending on how calcite precipitation rate varies throughout the year. The structure of the composite seasonal $\delta^{13}C$, Mg/Ca, Sr/Ca, and Ba/Ca cycles are very similar to one another, as evidenced by the strong positive correlations between the different proxies (Table 1). $\delta^{13}C$, Sr/Ca, and Ba/Ca values are lowest in increment 4 and highest in increment 10 and are therefore slightly offset from the Mg/Ca values which are at a minimum in increment 5 (May), and maximum values in increment 11. U/Ca values anti-correlate with Mg/Ca, Sr/Ca, Ba/Ca, and $\delta^{13}C$, and positively correlate with $\delta^{18}O$ (Table 1), with maximum values occurring in May.

5.5. Controls on annual geochemical cycles

The strong similarity in the composite annual Mg/Ca, Sr/Ca, Ba/Ca, and $\delta^{13}C$ cycles suggests a common control mechanism, the most likely of which is changes in the amount of CO_2 degassing and calcite precipitation which has occurred from the saturated drip water. Progressive CO_2 degassing leads to increases in solution and calcite $\delta^{13}C$ due to the preferential loss of ^{12}C in degassed CO_2. This degassing also drives calcite precipitation, which leads to increases in water and calcite Mg/Ca, Sr/Ca, and Ba/Ca ratios, because relevant partition coefficients (D) are significantly below 1 [15,18,39]. We suggest that seasonal variations in the amount of CO_2 degassing and calcite precipitation in Heshang Cave occur through two primary mechanisms, both related to rainfall and, hence, drip rate variations: (1) Prior calcite precipitation may occur within the epikarst or on the cave ceiling as stalactites. During drier periods, it has been suggested that low pCO_2 air pockets may exist in the epikarst [6]. If supersaturated groundwaters, in equilibrium with elevated soil pCO_2, encounter these air pockets, the solution will degas, leading to precipitation of calcite. Likewise, slower drip rates during dry periods may allow for more CO_2 degassing and calcite precipitation on the cave ceiling. (2) An alternative mechanism controlling the amount of CO_2 degassing and calcite precipitation may be a drip rate mechanism, in which the residence time of drip water on the stalagmite surface varies as drip rate varies throughout the year. During periods with low drip rates, the water may have more time to degas and precipitate calcite before it is displaced or diluted by subsequent drips. This second mechanism could generate seasonal cycles in the calcite even if the drip-water chemistry is relatively invariant throughout the year. Preliminary drip-water measurements reveal some seasonal variability in drip-water Mg/Ca ratios, indicating that varying degrees of prior calcite precipitation may be occurring during the year. The results of an ongoing cave environment and drip-water monitoring study will determine the relative role of these different mechanisms [47]. In any case, both the prior precipitation and drip-rate mechanisms lead to higher Mg/Ca, Sr/Ca, Ba/Ca, and $\delta^{13}C$ during dry periods, so that these measurements may provide a proxy for past monsoon rainfall.

The use of $\delta^{13}C$ and Mg/Ca, Sr/Ca, and Ba/Ca as proxies for rainfall is supported through comparison with modern rainfall and drip rate patterns (Fig. 2). There is very little rainfall between November and February (<50 mm/month) in the Heshang Cave region. This is therefore likely to be the period characterized by high Mg/Ca, Sr/Ca, Ba/Ca, and $\delta^{13}C$ values (increments 9–12), indicating a greater fraction of CO_2 degassing and calcite precipitation from saturated groundwaters at this time. Following these dry months, rainfall begins to increase, decreasing the fraction of CO_2 degassing and calcite precipitation, and hence decreasing Mg/Ca, Sr/Ca, Ba/Ca, and $\delta^{13}C$ in subsequent growth increments. With the onset of the summer monsoon in May (growth increment 5), when the lowest Mg/Ca values are observed, we propose that the fraction of calcite that precipitates may decrease considerably. This might even lead to a decrease in the linear growth rate of the stalagmite so that increments 5 and 6 represent a period of slower growth.

The composite U/Ca and $\delta^{18}O$ cycles are also consistent with this interpretation. U/Ca and $\delta^{18}O$ maxima occur during May, coincident with the summer monsoon onset. The $\delta^{18}O$ maximum at this time may represent heavier winter rain which is flushed rapidly into the cave. Following this, the drip water is isotopically lighter for the next several months, consisting largely of the summer monsoon rainfall. The $\delta^{18}O$ again begins increasing following the rise in heavy $\delta^{18}O$ rainfall early in the year (Fig. 3), until the maximum value is reached in May. The composite U/Ca cycle may also directly reflect variations in prior calcite precipitation (Fig. 7). While less is known about U partitioning into calcite, it is likely that $D \ll 1$ [40–42]. Despite this, U/Ca responds to prior calcite precipitation in the opposite sense to the other trace elements. This may be due to the close association between U (as uranyl ions) and P (as phosphate ions) observed in natural groundwaters [43,44]. It is known that P is strongly scavenged from groundwater during calcite precipitation [2]. Therefore, with increased prior calcite precipitation, we would expect decreased P/Ca ratios in the remaining drip water and hence in speleothem calcite. It is likely that U is scavenged along with P, leading to a similar pattern, governed by scavenging on to mineral surfaces rather than by the partition coefficient. The U/Ca maximum also coincides with the dark part of the annual band that contains high concentrations of organic material, which U and P are known to be associated with. This may be an additional mechanism controlling seasonal U/Ca (and P/Ca) variations.

5.6. Calcite precipitation model

Due to the numerous mechanisms that may affect speleothem trace-element and carbon-isotope composition, it is useful to utilize simple models to assess whether all of the observed variation could be easily explained by calcite precipitation alone. We have utilized three separate models which describe, in turn, how Mg/Ca, Sr/Ca, and $\delta^{13}C$ values of instantaneously precipitated calcite vary with progressive CO_2 degassing and calcite precipitation. A simple Rayleigh fractionation model is used to describe the increase in Mg/Ca (Fig. 8A) and Sr/Ca ratios in the solution, and hence in the calcite, with progressive calcite removal. The model is sensitive to changes of the partition coefficients, D_{Mg} and D_{Sr}, and initial Mg/Ca and Sr/Ca of the solution. $\delta^{13}C$ fractionation is also a Rayleigh process, with ^{12}C preferentially removed in degassed CO_2, thus increasing $\delta^{13}C$ in the remaining solution. Modelling this process is more complicated, though, because pH changes which accompany CO_2 degassing, alter the equilibrium distribution of the carbonate species and, therefore, also alter the $\delta^{13}C$ of HCO_3^- and the precipitated calcite [31,36]. This problem therefore must be solved iteratively, so we utilized a modified version of the PHREEQC-2 example of Appello [45] to describe the evolution of $\delta^{13}C$ in calcite precipitated from a supersaturated solution with pH = 7 (Fig. 8B). This model is quite flexible, allowing manipulation of several parameters, including the initial $\delta^{13}C$ values and the rate of CO_2 degassing, two parameters which can significantly alter the model results.

We use the models to address the question of whether the observed X/Ca-$\delta^{13}C$ relationship (where X = Mg or Sr) could be produced simply through progressive CO_2 degassing and precipitation of calcite. We first investigated the sensitivity of the models to different combinations of initial X/Ca value, initial fluid $\delta^{13}C$ value, temperature, D values, and CO_2 degassing rates. Based on the results of these, it is apparent that while a positive correlation should always be expected between X/Ca and $\delta^{13}C$ if CO_2 degassing and calcite precipitation are the dominant control mechanisms, the relationship can

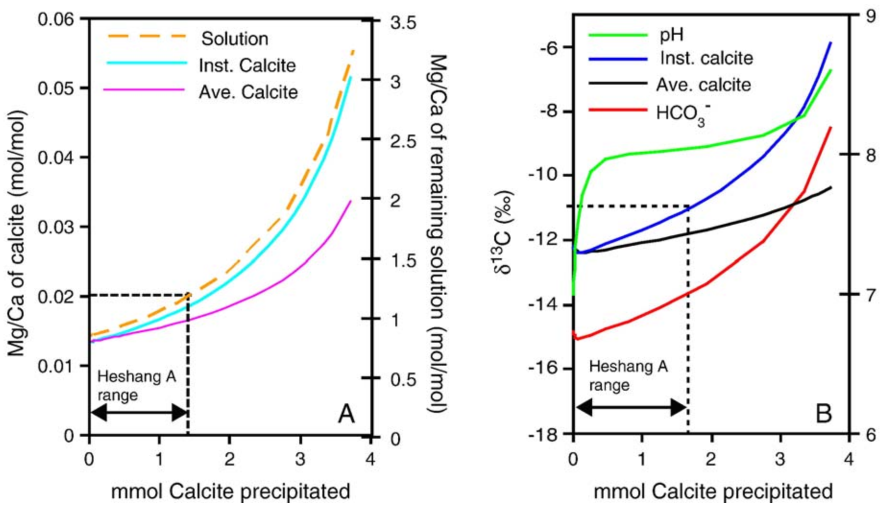

Fig. 8. The modelled evolution of (A) Mg/Ca ratios, and (B) $\delta^{13}C$ and pH as CO_2 degassing and calcite precipitation progressively removes C and Ca from a saturated solution which initially contained 5 mmol Ca. In (A), the evolution of Mg/Ca ratios in the instantaneous precipitate, the average precipitate, and the solution is shown. This model used an initial Mg/Ca = 0.84. In (B), the evolution of solution pH, $\delta^{13}C$ of solution HCO_3^-, and the $\delta^{13}C$ of instantaneous (or actual) precipitate and the average (or cumulative) calcite is shown. This model run utilized an initial $\delta^{13}C_{TDIC} = -16.75‰$, $T = 18$ °C, and a slow CO_2 degassing rate.

range from a quasi-linear one, with varying slopes and intercepts, to a highly exponential one, depending on the chosen boundary conditions. Initial fluid X/Ca values can affect both the effective slope and intercept of the X/Ca-$\delta^{13}C$ relationship (Fig. 9A). Altering the initial $\delta^{13}C$ value will affect the intercept, but not the slope. Increasing the *D* value will also increase both the slope and intercept, while increasing the CO_2 degassing rate will alter the relationship from fairly linear to quite exponential (Fig. 9B). The latter is the result of CO_2 degassing outpacing calcite precipitation at higher degassing rates.

To test if the model is able to reproduce the Heshang data using realistic boundary conditions, we set the temperature to 18 °C, equal to the mean cave temperature, and the initial Ca concentration to 5 mmol/l, so that the solution is saturated with respect to calcite. For the $\delta^{13}C$ model, we used a slow degassing rate, in which calcite precipitation keeps pace with CO_2 degassing. As in Appelo [45], the calcite precipitation and CO_2 degassing rates were set so that equilibrium with the final CO_2 pressure (10^{-4} atm) and with calcite saturation were reached concurrently. While this equilibrium situation may not apply to the majority of cave systems, it has been documented for certain locations [46]. Very fast degassing may often occur in caves, however, leading to kinetic fractionation of carbon isotopes [37]. For the Mg/Ca model, we used the lowest measured drip-water Mg/Ca ratio of 0.84 [47] as the initial value. This Mg/Ca ratio represents the maximum value possible for the initial composition. Lower values are possible if some prior calcite precipitation has occurred in the karst or on the cave roof. We then tuned D_{Mg} and initial fluid $\delta^{13}C$ until we achieved a good fit with the Mg–Ca and $\delta^{13}C$ data. The resulting boundary conditions we used are $D_{Mg}=0.016$ and initial $\delta^{13}C=-16.75$‰. The D_{Mg} value is within the range of expected *D* values given the temperature range in the cave and the published *D* values [11], although it is lower than expected for the mean cave temperature. This possibly reflects that more calcite precipitation occurs during the cooler periods, consistent with our suggestion that speleothem growth rates may slow down during the summer monsoon. Likewise, the initial $\delta^{13}C$ value is within the range expected for saturated cave waters which formed under open-system conditions, where bedrock dissolution took place in the presence of CO_2 with $\delta^{13}C \approx -25$‰ [31,36]. The models show the simultaneous increase of calcite Mg/Ca and $\delta^{13}C$ values as CO_2 degasses and calcite precipitates (Fig. 9). Under these model conditions, the observed Mg/Ca values may be accounted for by the removal of approximately 0–30% of the initial Ca from the solution (0–1.5 mmol). If the signal is dominated by prior calcite precipitation during transport through the epikarst or on the cave ceiling, the stalagmite calcite $\delta^{13}C$ and Mg/Ca would evolve along the instantaneous pathway (Fig. 8). If the degree of CO_2 degassing and calcite precipitation is varying on stalagmite surfaces due to the drip-rate mechanism, the stalagmite calcite should vary along the average calcite pathway.

For the Sr/Ca model, the initial solution Sr/Ca value we used is 0.69 mmol/mol, again equal to the lowest measured drip-water value. In order to fit the data, we set

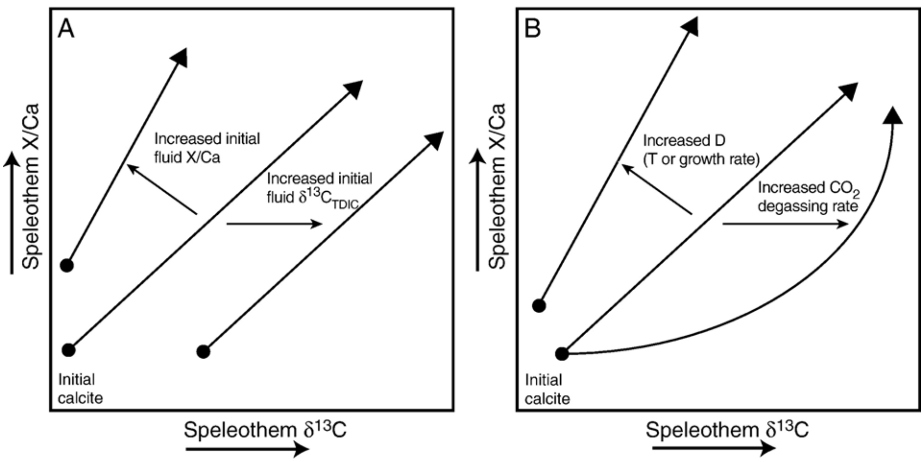

Fig. 9. Schematic of the trace element and $\delta^{13}C$ prior calcite precipitation model sensitivity. Progressive removal of Ca from a saturated solution, as precipitated $CaCO_3$ (calcite), will lead to progressive enrichment in X/Ca ratios (where X equals any element whose incorporation into calcite is governed by a partition coefficient, *D*, where $D<1$). This calcite precipitation is caused by degassing of CO_2 from the solution which drives the remaining solution and, hence, the precipitated calcite to higher $\delta^{13}C$. The resultant evolution of calcite chemistry is sensitive to changes in (A) initial fluid conditions, as well as (B) *D* values and CO_2 degassing rate.

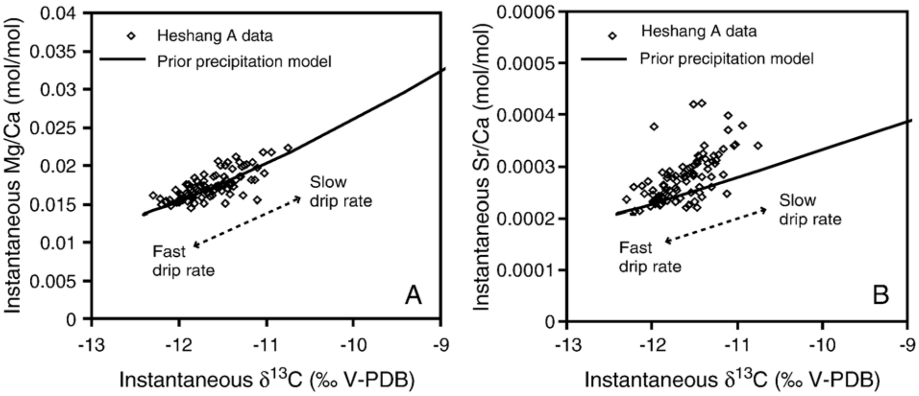

Fig. 10. Comparison of the micromilled Heshang data with the modelled co-evolution of instantaneous Mg/Ca (A) and Sr/Ca (B) values versus instantaneous δ^{13}C. For both models, we used the lowest measured Mg/Ca and Sr/Ca values, 0.84 mol/mol and 0.69 mmol/mol, respectively, as the initial starting point. We tuned the *D* values and the initial δ^{13}C value to achieve good fit. Following this prior calcite precipitation model, calcite with higher X/Ca and δ^{13}C values most likely formed during drier periods, when slower flow allowed for more CO_2 degassing and calcite precipitation.

$D_{Sr}=0.3$, which is rather high compared with other published values [11]. This value is not unrealistic, however, as D_{Sr} is known to be higher in waters with high Mg/Ca ratios [48], such as those at Heshang Cave. In addition, Sr incorporation into calcite is increased with increasing growth rates, which are also quite high in Heshang Cave speleothems (~300–400 μm/yr). In the case of both Mg and Sr, *D* values may be somewhat higher than those modelled if kinetic isotope effects due to rapid CO_2 degassing occur.

The good agreement between the instantaneous Mg/Ca and δ^{13}C data and the model (Fig. 10A), while not ruling out the possibility of other controlling factors, does indicate that the entire range of variability could be produced by varying amounts of prior calcite precipitation. The results of the instantaneous Sr/Ca–δ^{13}C model do not fit the data as well, suggesting other controls in addition to prior calcite precipitation (Fig. 10B). The scatter around the lines may have several causes, the most likely of which are: (1) variations in *D* values due to changes in temperature (D_{Mg}), growth rate (D_{Sr}), or solution Mg/Ca (D_{Sr}); and/or (2) variations in the drip rate mechanism in which case the calcite would evolve along the average calcite pathway rather than the instantaneous pathway. In both cases, however, higher Mg/Ca, Sr/Ca, and δ^{13}C values reflect drier periods, with slow drip rates and long transit times through the epikarst allowing for more CO_2 degassing and calcite precipitation en route to the stalagmite or on the stalagmite surface.

6. Conclusions

We report the presence of seasonal cycles in trace-element (Mg/Ca, Sr/Ca, Ba/Ca, and U/Ca) and stable-isotope (δ^{18}O and δ^{13}C) composition in a stalagmite, HS-4, collected from Heshang Cave, China. In a composite record, constructed by stacking 6 well-defined annual cycles, we observe a very strong positive correlation between Mg/Ca, Sr/Ca, Ba/Ca, and δ^{13}C in this sample. Through the use of simple models, we show that the measured Mg/Ca–δ^{13}C and Sr–Ca–δ^{13}C relationships can largely be accounted for through seasonal variations in the degree of CO_2 degassing and calcite precipitation that occurs from saturated drip waters. Such precipitation may occur as prior calcite precipitation in the epikarst or on the cave ceilings or by a drip-rate mechanism whereby variations in drip rate lead to variations in the degree of CO_2 degassing and calcite precipitation on the stalagmite surface. Both mechanisms lead to higher trace-element ratios and δ^{13}C during drier periods. Secondary controls on trace-element and isotope composition may include temperature, growth rate, and water chemistry.

δ^{18}O variations reflect variations in cave temperature and drip-water composition, both of which lead to maximum values during May, at the time of the summer monsoon onset. This provides a useful chronological marker in addition to a paleomonsoon and/or paleotemperature proxy in its own right. U/Ca values are anticorrelated with the other trace elements, possibly due to scavenging onto calcite crystal surfaces during prior precipitation.

This study has demonstrated that, through the use of δ^{18}O as an annual time marker, and the combined use of trace-element and stable-isotope measurements at high spatial resolution, reconstruction of seasonal rainfall at Heshang Cave should be possible. This would allow an assessment of changes in the behaviour of the East

Asian monsoon system at sub-annual resolution for the entire 9.5 kyr growth history of HS-4.

Acknowledgements

This work was supported by the Gary Comer Abrupt Climate Change Fellowship and NERC grant NE/B503925/1. We thank Ian Fairchild for useful discussions and comments on the manuscript.

References

[1] M.S. Roberts, P.L. Smart, A. Baker, Annual trace element variations in a Holocene speleothem, Earth Planet. Sci. Lett. 154 (1–4) (1998) 237–246.

[2] H.M. Huang, I.J. Fairchild, A. Borsato, S. Frisia, N.J. Cassidy, F. McDermott, C.J. Hawkesworth, Seasonal variations in Sr, Mg and P in modern speleothems (Grotta di Ernesto, Italy), Chem. Geol. 175 (3–4) (2001) 429–448.

[3] P. Treble, J.M.G. Shelley, J. Chappell, Comparison of high resolution sub-annual records of trace elements in a modern (1911–1992) speleothem with instrumental climate data from southwest Australia, Earth Planet. Sci. Lett. 216 (1–2) (2003) 141–153.

[4] I.J. Fairchild, A. Baker, A. Borsato, S. Frisia, R.W. Hinton, F. McDermott, A.F. Tooth, Annual to sub-annual resolution of multiple trace-element trends in speleothems, J. Geol. Soc. 158 (2001) 831–841.

[5] I.J. Fairchild, C.L. Smith, A. Baker, L. Fuller, C. Spotl, D.P. Mattey, F. McDermott and EIMF, Modification and preservation of environmental signals in speleothems, Earth Science Reviews, submitted 2005.

[6] I.J. Fairchild, A. Borsato, A.F. Tooth, S. Frisia, C.J. Hawkesworth, Y.M. Huang, F. McDermott, B. Spiro, Controls on trace element (Sr–Mg) compositions of carbonate cave waters: implications for speleothem climatic records, Chem. Geol. 166 (3– 4) (2000) 255–269.

[7] A.F. Tooth, I.J. Fairchild, Soil and karst aquifer hydrological controls on the geochemical evolution of speleothem-forming drip waters, Crag Cave, southwest Ireland, J. Hydrol. 273 (1–4) (2003) 51–68.

[8] P. Treble, J. Chappell, M.K. Gagan, K. McKeegan, T.M. Harrison, In situ measurement of seasonal $\delta^{18}O$ variations and analysis of isotopic trends in a modern speleothem from southwest Australia, Earth Planet. Sci. Lett. 233 (2005) 17–32.

[9] S. Verheyden, E. Keppens, I.J. Fairchild, F. McDermott, D. Weis, Mg, Sr and Sr isotope geochemistry of a Belgian Holocene speleothem; implications for paleoclimate reconstructions, in: D. Weis, D.J. DePaolo (Eds.), Isotope Tracers in Geochemistry and Cosmochemistry [modified], vol. 169, Elsevier, Amsterdam, 2000, pp. 131–144.

[10] M. Gascoyne, Trace element partition coefficients in the calcite–water system and their palaeoclimatic significance in cave studies, J. Hydrol. 61 (1983) 231.

[11] Y.M. Huang, I.J. Fairchild, Partitioning of Sr^{2+} and Mg^{2+} into calcite under karst-analogue experimental conditions, Geochim. Cosmochim. Acta 65 (1) (2001) 47–62.

[12] T.M.L. Wigley, M.C. Brown, The physics of caves, in: T.D. Ford, C.H.D. Cullingford (Eds.), The Science of Speleology, Academic Press, London, 1976, pp. 329–358.

[13] D.W. Cowell, D.C. Ford, Hydrochemistry of a dolomite karst: the Bruce Peninsula of Ontario, Can. J. Earth Sci. 17 (1980) 520–526.

[14] K. Chou, R.M. Garrels, R. Wollast, Comparative study of the kinetics and mechanisms of dissolution of carbonate minerals, Chem. Geol. 78 (1989) 269–282.

[15] J.W. Morse, M.L. Bender, Partition coefficients in calcite: examination of factors influencing the validity of experimental results and their application to natural systems, Chem. Geol. 82 (1990) 265–277.

[16] E. Busenberg, L.N. Plummer, The kinetics of dissolution of dolomite in CO_2–H_2O systems at 1.5 to 65 °C and 0 to 1 atm P_{CO_2}, Am. J. Sci. 282 (1982) 45–78.

[17] M.R. McGillen, I.J. Fairchild, An experimental study of incongruent dissolution of $CaCO_3$ under analogue glacial conditions, Journal of Glaciology (in press).

[18] D.W. Lea, H.J. Spero, Assessing the reliability of paleochemical tracers – barium uptake in the shells of planktonic foraminifera, Paleoceanography 9 (3) (1994) 445–452.

[19] G.J. Bowen, L.I. Wassenaar, K.A. Hobson, Global application of stable hydrogen and oxygen isotopes to wildlife forensics, Oecologia 143 (3) (2005) 337–348.

[20] G.J. Bowen, J. Revenaugh, Interpolating the isotopic composition of modern meteoric precipitation, Water Resour. Res. 39 (10) (2003).

[21] W. Dansgaard, Stable isotopes in precipitation, Tellus 16 (1964) 436–438.

[22] K.R. Johnson, B.L. Ingram, Spatial and temporal variability in the stable isotope systematics of modern precipitation in China: implications for paleoclimate reconstructions, Earth Planet. Sci. Lett. 220 (3–4) (2004) 365–377.

[23] D.W. Lea, P.A. Martin, A rapid mass spectrometric method for the simultaneous analysis of barium, cadmium, and strontium in foraminifera shells, Geochim. Cosmochim. Acta 60 (16) (1996) 3143–3149.

[24] Y. Rosenthal, M.P. Field, R.M. Sherrell, Precise determination of element/calcium ratios in calcareous samples using sector field inductively coupled plasma mass spectrometry, Anal. Chem. 71 (1999) 3248–3253.

[25] C.A. Craig, K.E. Jarvis, L.J. Clarke, An assessment of calibration strategies for the quantitative and semi-quantitative analysis of calcium carbonate matrices by laser ablation–inductively coupled plasma–mass spectrometry (LA–ICP–MS), Journal of Analytical Atomic Spectrometry 15 (8) (2000) 1001–1008.

[26] R.E. Russo, X.L. Mao, H.C. Liu, J. Gonzalez, S.S. Mao, Laser ablation in analytical chemistry – a review, Talanta 57 (3) (2002) 425–451.

[27] K.R. Johnson, N.S. Belshaw, G.M. Henderson, LA-MC-ICPMS measurement of trace element/calcium ratios in speleothem calcite, in prep.

[28] D.X. Yuan, H. Cheng, R.L. Edwards, C.A. Dykoski, M.J. Kelly, M.L. Zhang, J.M. Qing, Y.S. Lin, Y.J. Wang, J.Y. Wu, J.A. Dorale, Z.S. An, Y.J. Cai, Timing, duration, and transitions of the Last Interglacial Asian Monsoon, Science 304 (5670) (2004) 575–578.

[29] D. Fleitmann, S.J. Burns, M. Mudelsee, U. Neff, J. Kramers, A. Mangini, A. Matter, Holocene forcing of the Indian monsoon recorded in a stalagmite from Southern Oman, Science 300 (5626) (2003) 1737–1739.

[30] D. Genty, A. Baker, B. Vokal, Intra- and inter-annual growth rate of modern stalagmites, Chem. Geol. 176 (1–4) (2001) 191–212.

[31] C.H. Hendy, The isotopic geochemistry of speleothems: Part 1. The calculation of the effects of different modes of formation on

the isotopic composition of speleothems and their applicability as paleoclimatic indicators, Geochim. Cosmochim. Acta 35 (1971) 805–824.
[32] R.F. Denniston, L.A. Gonzalez, Y. Asmerom, M.K. Reagan, H. Recelli-Snyder, Speleothem carbon isotopic records of Holocene environments in the Ozark Highlands, USA, Quat. Int. 67 (2000) 21–27.
[33] J.A. Dorale, L.A. Gonzalez, M.K. Reagan, D.A. Pickett, M.T. Murrell, R.G. Baker, A high-resolution record of Holocene climate change in speleothem calcite from cold water cave, Northeast Iowa, Science 258 (5088) (1992) 1626–1630.
[34] J.A. Dorale, R.L. Edwards, E. Ito, L.A. Gonzalez, Climate and vegetation history of the midcontinent from 75 to 25 ka: a speleothem record from Crevice Cave, Missouri, USA, Science 282 (5395) (1998) 1871–1874.
[35] A. Baker, E. Ito, P.L. Smart, R.F. McEwan, Elevated and variable values of C-13 in speleothems in a British cave system, Chem. Geol. 136 (3–4) (1997) 263–270.
[36] M. Dulinski, K. Rozanski, Formation of C-13 C-12 isotope ratios in speleothems – a semidynamic model, Radiocarbon 32 (1) (1990) 7–16.
[37] C. Spotl, I.J. Fairchild, A.F. Tooth, Cave air control on dripwater geochemistry, Obir Caves (Austria): implications for speleothem deposition in dynamically ventilated caves, Geochim. Cosmochim. Acta 69 (10) (2005) 2451–2468.
[38] S. Verheyden, E. Keppens, I.J. Fairchild, F. McDermott, D. Weis, Mg, Sr and Sr isotope geochemistry of a Belgian Holocene speleothem: implications for paleoclimate reconstructions, Chem. Geol. 169 (1–2) (2000) 131–144.
[39] J. Pingitore, E. Nicholas, M.P. Eastman, The experimental partitioning of Ba^{2+} into calcite, Chem. Geol. 45 (1–2) (1984) 113–120.
[40] D.E. Meece, L.K. Benninger, The coprecipitation of Pu and other radionuclides with $CaCO_3$, Geochim. Cosmochim. Acta 57 (1992) 1447–1458.
[41] A.D. Russell, S. Emerson, B.K. Nelson, J. Erez, D.W. Lea, Uranium in foraminiferal calcite as a recorder of seawater uranium concentrations, Geochim. Cosmochim. Acta 58 (2) (1994) 671–681.
[42] Y. Kitano, T. Oomori, The coprecipitation of uranium with calcium carbonate, J. Oceanogr. Soc. Japan 27 (1) (1971) 34–42.
[43] A. Sanding, J. Bruno, The solubility of $(UO_2)_3(PO_4)_2 \cdot 4H_2O(s)$ and the formation of U(VI) phosphate complexes: their influence in uranium speciation in natural waters, Geochim. Cosmochim. Acta 56 (12) (1992) 4135–4145.
[44] J.L. Jerden, A.K. Sinha, Phosphate based immobilization of uranium in an oxidizing bedrock aquifer, Appl. Geochem. 18 (6) (2003) 823–843.
[45] C.A.J. Appelo, Calculating the fractionation of isotopes in hydrochemical (transport) processes with PHREEQC-2, in: H.D. Schultz, A. Hadeler (Eds.), Geochemical Processes in Soil and Groundwater, Wiley-VCH, GeoProc 2002, 2002, pp. 383–398.
[46] M. Bar-Matthews, A. Ayalon, A. Matthews, E. Sass, L. Halicz, Carbon and oxygen isotope study of the active water–carbonate system in a karstic Mediterranean cave: implications for paleoclimate research in semiarid regions, Geochim. Cosmochim. Acta 60 (2) (1996) 337–347.
[47] C.Y. Hu, K.R. Johnson, G.M. Henderson, Modern trace-element and stable isotope systematics in Heshang Cave, China: implications for paleomonsoon reconstruction, in prep.
[48] A. Mucci, J.W. Morse, The incorporation of Mg^{2+} and Sr^{2+} into calcite overgrowths – influences of growth-rate and solution composition, Geochim. Cosmochim. Acta 47 (2) (1983) 217–233.